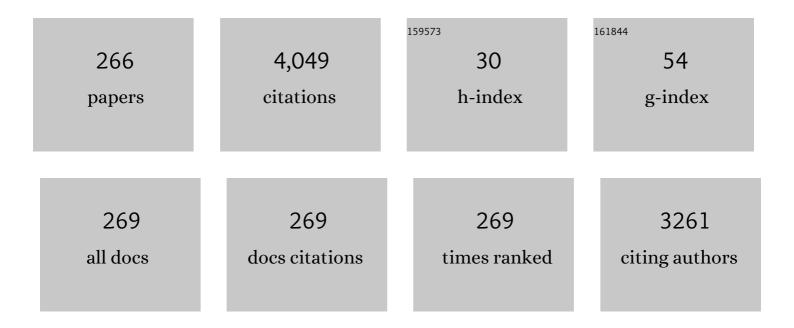
Qing-An Huang

List of Publications by Year in descending order

Source: https://exaly.com/author-pdf/2704382/publications.pdf Version: 2024-02-01



#	Article	IF	CITATIONS
1	Analysis and design of polysilicon thermal flexure actuator. Journal of Micromechanics and Microengineering, 1999, 9, 64-70.	2.6	309
2	Metal oxide semiconductor nanomembrane–based soft unnoticeable multifunctional electronics for wearable human-machine interfaces. Science Advances, 2019, 5, eaav9653.	10.3	213
3	<italic>LC</italic> Passive Wireless Sensors Toward a Wireless Sensing Platform: Status, Prospects, and Challenges. Journal of Microelectromechanical Systems, 2016, 25, 822-841.	2.5	177
4	A novel capacitive-type humidity sensor using CMOS fabrication technology. Sensors and Actuators B: Chemical, 2004, 99, 491-498.	7.8	128
5	A modified cellular automata algorithm for the simulation of boundary advancement in deposition topography simulation. Journal of Micromechanics and Microengineering, 2006, 16, 1-8.	2.6	117
6	Simultaneous Remote Sensing of Temperature and Humidity by LC-Type Passive Wireless Sensors. Journal of Microelectromechanical Systems, 2015, 24, 1117-1123.	2.5	103
7	An <italic>LC</italic> -Type Passive Wireless Humidity Sensor System With Portable Telemetry Unit. Journal of Microelectromechanical Systems, 2015, 24, 575-581.	2.5	101
8	A novel capacitive pressure sensor based on sandwich structures. Journal of Microelectromechanical Systems, 2005, 14, 1272-1282.	2.5	95
9	2-D Micromachined Thermal Wind Sensors—A Review. IEEE Internet of Things Journal, 2014, 1, 216-232.	8.7	88
10	High-Voltage Flexible Microsupercapacitors Based on Laser-Induced Graphene. ACS Applied Materials & Interfaces, 2018, 10, 26357-26364.	8.0	70
11	Extending the remote distance of LC passive wireless sensors via strongly coupled magnetic resonances. Journal of Micromechanics and Microengineering, 2014, 24, 125021.	2.6	69
12	A Passive Wireless Adaptive Repeater for Enhancing the Readout of LC Passive Wireless Sensors. IEEE Microwave and Wireless Components Letters, 2016, 26, 543-545.	3.2	63
13	Passive wireless integrated humidity sensor based on dualâ€layer spiral inductors. Electronics Letters, 2014, 50, 1287-1289.	1.0	61
14	Fabrication of a Micromachined Two-Dimensional Wind Sensor by Au–Au Wafer Bonding Technology. Journal of Microelectromechanical Systems, 2012, 21, 467-475.	2.5	59
15	A Fully Packaged CMOS Interdigital Capacitive Humidity Sensor With Polysilicon Heaters. IEEE Sensors Journal, 2011, 11, 2986-2992.	4.7	58
16	An analytical model for pull-in voltage of clamped–clamped multilayer beams. Sensors and Actuators A: Physical, 2004, 116, 15-21.	4.1	57
17	LC Wireless Sensitive Pressure Sensors With Microstructured PDMS Dielectric Layers for Wound Monitoring. IEEE Sensors Journal, 2018, 18, 4886-4892.	4.7	57
18	Analytical modeling and optimization for a laterally-driven polysilicon thermal actuator. Microsystem Technologies, 1999, 5, 133-137.	2.0	55

#	Article	IF	CITATIONS
19	Improvement of the 2D dynamic CA method for photoresist etching simulation and its application to deep UV lithography simulations of SU-8 photoresists. Journal of Micromechanics and Microengineering, 2007, 17, 2538-2547.	2.6	53
20	Size and temperature dependence of Young's modulus of a silicon nano-plate. Journal Physics D: Applied Physics, 2008, 41, 165406.	2.8	53
21	A silicon directly bonded capacitive absolute pressure sensor. Sensors and Actuators A: Physical, 2007, 135, 507-514.	4.1	52
22	RF MEMS membrane switches on GaAs substrates for X-band applications. Journal of Microelectromechanical Systems, 2005, 14, 464-471.	2.5	49
23	Modeling, design and fabrication of a triple-layered capacitive pressure sensor. Sensors and Actuators A: Physical, 2005, 117, 71-81.	4.1	48
24	A Micromachined Inline-Type Wideband Microwave Power Sensor Based on GaAs MMIC Technology. Journal of Microelectromechanical Systems, 2009, 18, 705-714.	2.5	48
25	A cellular automaton-based simulator for silicon anisotropic etching processes considering high index planes. Journal of Micromechanics and Microengineering, 2007, 17, S38-S49.	2.6	43
26	DRIE Trenches and Full-Bridges for Improving Sensitivity of 2-D Micromachined Silicon Thermal Wind Sensor. Journal of Microelectromechanical Systems, 2017, 26, 1073-1081.	2.5	42
27	Implementation of Multiparameter Monitoring by an <italic>LC</italic> -Type Passive Wireless Sensor Through Specific Winding Stacked Inductors. IEEE Internet of Things Journal, 2015, 2, 168-174.	8.7	36
28	Flip-Chip Packaging for a Two-Dimensional Thermal Flow Sensor Using a Copper Pillar Bump Technology. IEEE Sensors Journal, 2007, 7, 990-995.	4.7	35
29	A Cross-Type Thermal Wind Sensor With Self-Testing Function. IEEE Sensors Journal, 2010, 10, 340-346.	4.7	34
30	A Novel Three-State RF MEMS Switch for Ultrabroadband (DC-40 GHz) Applications. IEEE Electron Device Letters, 2013, 34, 1062-1064.	3.9	33
31	A monolithic integrated ultra-flexible all-solid-state supercapacitor based on a polyaniline conducting polymer. Journal of Materials Chemistry A, 2019, 7, 15378-15386.	10.3	33
32	Low Cost Paper-Based LC Wireless Humidity Sensors and Distance-Insensitive Readout System. IEEE Sensors Journal, 2019, 19, 4717-4725.	4.7	32
33	Numerical simulation of a polysilicon thermal flexure actuator. Microsystem Technologies, 2002, 8, 17-21.	2.0	28
34	Macro-modeling for polysilicon cascaded bent beam electrothermal microactuators. Sensors and Actuators A: Physical, 2006, 128, 165-175.	4.1	28
35	A simple approach to characterizing the driving force of polysilicon laterally driven thermal microactuators. Sensors and Actuators A: Physical, 2000, 80, 267-272.	4.1	27
36	A microwave power sensor based on GaAs MMIC technology. Journal of Micromechanics and Microengineering, 2007, 17, 2132-2137.	2.6	27

#	Article	IF	CITATIONS
37	A FCOB packaged thermal wind sensor with compensation. Microsystem Technologies, 2010, 16, 511-518.	2.0	27
38	Micromachining of Pyrex 7740 Glass by Silicon Molding and Vacuum Anodic Bonding. Journal of Microelectromechanical Systems, 2011, 20, 909-915.	2.5	26
39	Development of a self-packaged 2D MEMS thermal wind sensor for low power applications. Journal of Micromechanics and Microengineering, 2015, 25, 085011.	2.6	26
40	The influence of surface effects on size-dependent mechanical properties of silicon nanobeams at finite temperature. Journal Physics D: Applied Physics, 2009, 42, 045409.	2.8	25
41	Enhanced performance of a CMOS interdigital capacitive humidity sensor by graphene oxide. , 2011, , .		24
42	A novel 2D dynamic cellular automata model for photoresist etching process simulation. Journal of Micromechanics and Microengineering, 2005, 15, 652-662.	2.6	23
43	Modeling, simulation and experimental verification of inclined UV lithography for SU-8 negative thick photoresists. Journal of Micromechanics and Microengineering, 2008, 18, 125017.	2.6	23
44	Sensitivity Improvement of a 2D MEMS Thermal Wind Sensor for Low-Power Applications. IEEE Sensors Journal, 2016, 16, 4300-4308.	4.7	23
45	Effect of Die-Bonding Process on MEMS Device Performance: System-Level Modeling and Experimental Verification. Journal of Microelectromechanical Systems, 2009, 18, 274-286.	2.5	22
46	Symmetric LC Circuit Configurations for Passive Wireless Multifunctional Sensors. Journal of Microelectromechanical Systems, 2019, 28, 344-350.	2.5	22
47	A micromachined silicon capacitive temperature sensor for wide temperature range applications. Journal of Micromechanics and Microengineering, 2010, 20, 055036.	2.6	21
48	Modeling of Temperature Effects on Micromachined Silicon Thermal Wind Sensors. Journal of Microelectromechanical Systems, 2015, 24, 2033-2039.	2.5	21
49	Young's modulus of silicon nanoplates at finite temperature. Applied Surface Science, 2008, 255, 2449-2455.	6.1	20
50	Novel DC-40GHz MEMS series-shunt switch for high isolation and high power applications. Sensors and Actuators A: Physical, 2014, 214, 101-110.	4.1	20
51	A physical model for silicon anisotropic chemical etching. Semiconductor Science and Technology, 2005, 20, 524-531.	2.0	19
52	Effect of native oxides on the elasticity of a silicon nano-scale beam. Solid State Communications, 2008, 145, 351-354.	1.9	19
53	Modeling and Simulations of Anisotropic Etching of Silicon in Alkaline Solutions with Experimental Verification. Journal of the Electrochemical Society, 2009, 156, F29.	2.9	19
54	Lateral Contact Three-State RF MEMS Switch for Ground Wireless Communication by Actuating Rhombic Structures. Journal of Microelectromechanical Systems, 2013, 22, 10-12.	2.5	19

#	Article	IF	CITATIONS
55	An <italic>LC</italic> Passive Wireless Multifunctional Sensor Using a Relay Switch. IEEE Sensors Journal, 2016, 16, 4968-4973.	4.7	19
56	Enhancing the Remote Distance of <i>LC</i> Passive Wireless Sensors by Parity-Time Symmetry Breaking. Physical Review Applied, 2020, 13, .	3.8	19
57	A Novel 3-D Dynamic Cellular Automata Model for Photoresist-Etching Process Simulation. IEEE Transactions on Computer-Aided Design of Integrated Circuits and Systems, 2007, 26, 100-114.	2.7	18
58	Pull-in characterization of doubly-clamped composite beams. Sensors and Actuators A: Physical, 2009, 151, 118-126.	4.1	18
59	Gamma and electron beam irradiation effects on the resistance of micromachined polycrystalline silicon beams. Sensors and Actuators A: Physical, 2012, 177, 99-104.	4.1	18
60	Effect of Environmental Humidity on Dielectric Charging Effect in RF MEMS Capacitive Switches Based on \$C\$– \$V\$ Properties. Journal of Microelectromechanical Systems, 2013, 22, 637-645.	2,5	18
61	Octagon-Shaped 2-D Micromachined Thermal Wind Sensor for High-Accurate Applications. Journal of Microelectromechanical Systems, 2018, 27, 739-747.	2.5	18
62	Field emission from the surface quantum well of silicon. Applied Surface Science, 1996, 93, 77-83.	6.1	17
63	A Cyclic Scanning Repeater for Enhancing the Remote Distance of LC Passive Wireless Sensors. IEEE Transactions on Circuits and Systems I: Regular Papers, 2016, 63, 1426-1433.	5.4	17
64	Effect of Insulation Trenches on Micromachined Silicon Thermal Wind Sensors. IEEE Sensors Journal, 2017, 17, 8324-8331.	4.7	17
65	Instability of field emission from silicon covered with a thin oxide due to electron trapping. Journal of Applied Physics, 1996, 79, 3703-3707.	2.5	16
66	Field emission from surface states of silicon. Journal of Applied Physics, 1997, 81, 7589-7594.	2.5	16
67	A nodal analysis method for simulating the behavior of electrothermal microactuators. Microsystem Technologies, 2007, 14, 119-129.	2.0	16
68	A 2D Wind Sensor Using the <inline-formula> <tex-math notation="LaTeX">\$Delta\$ </tex-math> </inline-formula> P Thermal Feedback Control. Journal of Microelectromechanical Systems, 2018, 27, 377-379.	2.5	16
69	Field emission from a silicon surface potential well through a thin oxide. Journal of Applied Physics, 1995, 78, 6770-6774.	2.5	13
70	An online test microstructure for thermal conductivity of surface-micromachined polysilicon thin films. IEEE Sensors Journal, 2006, 6, 428-433.	4.7	13
71	Measurement of residual stress in multilayered thin films by a full-field optical method. Sensors and Actuators A: Physical, 2006, 126, 93-97.	4.1	13
72	Gamma Irradiation Effects on Surface-Micromachined Polysilicon Resonators. Journal of Microelectromechanical Systems, 2011, 20, 1071-1073.	2,5	13

#	Article	IF	CITATIONS
73	Humidity sensing properties of the sensor based on graphene oxide films with different dispersion concentrations. , 2011, , .		12
74	Effects of Ambient Humidity on a Micromachined Silicon Thermal Wind Sensor. Journal of Microelectromechanical Systems, 2014, 23, 253-255.	2.5	12
75	Experimental Study of the Bending Effect on <italic>LC</italic> Wireless HumiditySensors Fabricated on Flexible PET Substrates. Journal of Microelectromechanical Systems, 2018, 27, 761-763.	2.5	12
76	Observation of the perturbed eigenvalues of PT-symmetric LC resonator systems. Journal of Physics Communications, 2021, 5, 045010.	1.2	12
77	A system-level model for a silicon thermal flow sensor. Microsystem Technologies, 2009, 15, 279-285.	2.0	11
78	Influence of environmental temperature on the dynamic properties of a die attached MEMS device. Microsystem Technologies, 2009, 15, 925-932.	2.0	11
79	Modelling of the elastic properties of crystalline silicon using lattice dynamics. Journal Physics D: Applied Physics, 2011, 44, 335401.	2.8	11
80	A simple method for extracting material parameters of multilayered MEMS structures using resonance frequency measurements. Journal of Micromechanics and Microengineering, 2014, 24, 075014.	2.6	11
81	A Simple Extraction Method of Young's Modulus for Multilayer Films in MEMS Applications. Micromachines, 2017, 8, 201.	2.9	11
82	Comprehensive Simulations for Ultraviolet Lithography Process of Thick SU-8 Photoresist. Micromachines, 2018, 9, 341.	2.9	11
83	Multi-Parameters Detection Implemented by LC Sensors With Branching Inductors. IEEE Sensors Journal, 2019, 19, 304-310.	4.7	11
84	Parallelized Wireless Sensing System for Continuous Monitoring of Microtissue Spheroids. ACS Sensors, 2020, 5, 2036-2043.	7.8	11
85	A field-enhanced generation model for field emission from p-type silicon. IEEE Electron Device Letters, 1997, 18, 616-618.	3.9	10
86	Large-signal lumped-parameter macromodels for the equivalent circuit representation of electromechanical transducers. Journal of Micromechanics and Microengineering, 2004, 14, 452-461.	2.6	10
87	Effect of temperature and elastic constant on the piezoresistivity of silicon nanobeams. Journal of Applied Physics, 2009, 105, 086102.	2.5	10
88	An Efficient Simulation System for Inclined UV Lithography Processes of Thick SU-8 Photoresists. IEEE Transactions on Semiconductor Manufacturing, 2011, 24, 294-303.	1.7	10
89	Temperature Effects on the Wind Direction Measurement of 2D Solid Thermal Wind Sensors. Sensors, 2015, 15, 29871-29881.	3.8	10
90	Laterally-actuated inside-driven RF MEMS switches fabricated by a SOG process. Journal of Micromechanics and Microengineering, 2015, 25, 065007.	2.6	10

#	Article	IF	CITATIONS
91	Experiment of the MEMS Wind Sensor Based on Temperature-Balanced Mode. IEEE Sensors Journal, 2017, 17, 2316-2317.	4.7	10
92	An Interdigital Capacitive Humidity Sensor With Layered Black Phosphorus Flakes as a Sensing Material. IEEE Sensors Journal, 2019, 19, 11007-11013.	4.7	10
93	Design and finite element analysis of weighted-stiffness microelectromechanical digital-to-analogue converters. Electronics Letters, 2001, 37, 755.	1.0	9
94	A simple method for measuring the thermal diffusivity of surface-micromachined polysilicon thin films. Journal of Micromechanics and Microengineering, 2006, 16, 981-985.	2.6	9
95	Orientation Effects in Ballistic High-Strained P-type Si Nanowire FETs. Sensors, 2009, 9, 2746-2759.	3.8	9
96	Hot-forming of micro glass cavities for MEMS wafer level hermetic packaging. , 2010, , .		9
97	A hot film wind sensor with four Constant Temperature Difference elements fabricated on ceramic substrate. , 2011, , .		9
98	Temperature sensing properties of the passive wireless sensor based on graphene oxide films. , 2014, , .		9
99	Effects of Metal Plane in LC Passive Wireless Sensors. , 2018, 2, 1-3.		9
100	Temperature Effects of a Ceramic MEMS Thermal Wind Sensor Based on a Temperature-Balanced Mode. IEEE Sensors Journal, 2019, 19, 7254-7260.	4.7	9
101	Modeling, Simulation, and Fabrication of a 2-D Anemometer Based on a Temperature-Balanced Mode. IEEE Sensors Journal, 2019, 19, 4796-4803.	4.7	9
102	Novel Anemometer Based on Inductor Bending Effect. Journal of Microelectromechanical Systems, 2019, 28, 321-323.	2.5	9
103	An Impedance Matching Method for LC Passive Wireless Sensors. IEEE Sensors Journal, 2020, 20, 13833-13841.	4.7	9
104	Analysis of electromagnetic interference of a capacitive RF MEMS switch during switching. Microsystem Technologies, 2008, 14, 349-360.	2.0	8
105	Modeling of H2O adsorption-induced curvature of a metal/silicon nanocantilever. Applied Surface Science, 2009, 255, 9404-9408.	6.1	8
106	Micromachining of Pyrex7740 glass and their applications to wafer-level hermetic packaging of MEMS devices. , 2010, , .		8
107	Strain Effect of the Dielectric Constant in Silicon Dioxide. Journal of Microelectromechanical Systems, 2010, 19, 1521-1523.	2.5	8
108	Modeling of silicon thermal expansion using strained phonon spectra. Journal of Micromechanics and Microengineering, 2012, 22, 085007.	2.6	8

6

#	Article	IF	CITATIONS
109	A New Method for Real-Time Measuring the Temperature-Dependent Dielectric Constant of the Silicone Oil. IEEE Sensors Journal, 2016, 16, 8792-8797.	4.7	8
110	A robust and low-power 2-D thermal wind sensor based on a glass-in-silicon reflow process. Microsystem Technologies, 2016, 22, 151-162.	2.0	8
111	A Generalized Polynomial Chaos-Based Approach to Analyze the Impacts of Process Deviations on MEMS Beams. Sensors, 2017, 17, 2561.	3.8	8
112	Applying Metamaterial-Based Repeater in LC Passive Wireless Sensors to Enhance Readout. IEEE Sensors Journal, 2018, 18, 1755-1760.	4.7	8
113	Temperature Effect and Its Compensation of a Micromachined 2-D Anemometer. IEEE Sensors Journal, 2019, 19, 5454-5459.	4.7	8
114	Configuration of a Self-Heated Double Wheatstone Bridge for 2-D Wind Sensors. Journal of Microelectromechanical Systems, 2019, 28, 125-130.	2.5	8
115	A nodal analysis method for electromechanical behavior simulation of bow-tie shaped microbeams. Microsystem Technologies, 2009, 15, 985-991.	2.0	7
116	A MEMS pressure sensor based on Hall effect. , 2011, , .		7
117	Design of LC-type passive wireless multi-parameter sensor. , 2013, , .		7
118	DRIE trenches and full-bridges design for sensitivity improvement of MEMS silicon thermal wind sensor. , 2017, , .		7
119	Analysis and Compensation of Benchmark Drift of Micromachined Thermal Wind Sensor Caused by Packaging Asymmetry. IEEE Transactions on Industrial Electronics, 2022, 69, 950-959.	7.9	7
120	Design and 3D modeling investigation of a microfluidic electrode array for electrical impedance measurement of single yeast cells. Electrophoresis, 2021, 42, 1996-2009.	2.4	7
121	A New Interpretation of the Orientation Effect in GaAs Metal Semiconductor Field Effect Transistors. Japanese Journal of Applied Physics, 1991, 30, L11-L14.	1.5	6
122	Field emission from a silicon surfaceâ€potential well based on an Airy function approach. Journal of Applied Physics, 1995, 78, 1254-1258.	2.5	6
123	Effect of (2 × 1) Surface Reconstruction on Elasticity of a Silicon Nano-Plate. Chinese Physics Letters, 2008, 25, 1403-1406.	3.3	6
124	Fullerene as electrical hinge. Applied Physics Letters, 2012, 100, 193111.	3.3	6
125	Large scale three-dimensional simulations for thick SU-8 lithography process based on a full hash fast marching method. Microelectronic Engineering, 2014, 123, 171-174.	2.4	6

A novel capacitive temperature sensor for a lab-on-a-chip system. , 2014, , .

8

#	Article	IF	CITATIONS
127	In-situ determination of the coefficient of thermal expansion of polysilicon thin films using micro-rotating structures. Thin Solid Films, 2014, 552, 184-191.	1.8	6
128	Flexible Passive Wireless Pressure and Moisture Dual-Parameter Sensor for Wound Monitoring. , 2018, , .		6
129	Three-Dimensional Simulation of DRIE Process Based on the Narrow Band Level Set and Monte Carlo Method. Micromachines, 2018, 9, 74.	2.9	6
130	Sensitivity Improvement of MEMS Thermal Wind Senor Using Vertical Stacking Thermistors. , 2019, , .		6
131	Modeling of Packaged MEMS Thermal Wind Sensor Operating on CP Mode. IEEE Transactions on Electron Devices, 2019, 66, 2375-2381.	3.0	6
132	Low-Drift MEMS Thermal Wind Sensor With Symmetric Packaging Using Plastic Injection Molding Process. IEEE Transactions on Instrumentation and Measurement, 2021, 70, 1-8.	4.7	6
133	Fabrication and Characterization of Flexible Capacitive Humidity Sensors Based on Graphene Oxide on Porous PTFE Substrates. Sensors, 2021, 21, 5118.	3.8	6
134	Field emission from silicon including continuum energy and surface quantization. Applied Surface Science, 1997, 119, 229-236.	6.1	5
135	A new micro-rotating structure. Journal of Physics: Conference Series, 2006, 34, 552-557.	0.4	5
136	In-line method for extracting the temperature coefficient of resistance of surface-micromachined polysilicon thin films. Sensors and Actuators A: Physical, 2007, 136, 249-254.	4.1	5
137	Theoretical study of electromechanical property in a p-type silicon nanoplate for mechanical sensors. Chinese Physics B, 2008, 17, 4292-4299.	1.4	5
138	A 3D profile simulator for inclined/multi-directional UV lithography process of negative-tone thick photoresists. , 2009, , .		5
139	A self-packaged two-dimensional thermal wind sensor based on thermopiles for low cost applications. Journal of Micromechanics and Microengineering, 2014, 24, 075008.	2.6	5
140	Effects of thermally induced packaging stress on a distributed RF MEMS phase shifter. Microsystem Technologies, 2015, 21, 869-874.	2.0	5
141	Parallel capacitive temperature microâ€sensor for passive wireless sensing applications. Electronics Letters, 2016, 52, 1345-1347.	1.0	5
142	Encapsulation glue Effect of Encapsulation Glue on Micromachined Thermal Wind Sensor. , 2018, 2, 1-3.		5
143	Ceramic Film Packaging for 2-D Thermal Wind Sensor Using LTCC Technology. Journal of Microelectromechanical Systems, 2019, 28, 1080-1087.	2.5	5
144	Fabrication of a Piezoresistive Barometric Pressure Sensor by a Silicon-on-Nothing Technology. Journal of Sensors, 2019, 2019, 1-10.	1.1	5

#	Article	IF	CITATIONS
145	Quadruple sensitivity improvement for wind speed sensor using dual-layer bended inductors. Sensors and Actuators A: Physical, 2020, 303, 111786.	4.1	5
146	A high-throughput microfluidic diploid yeast long-term culturing (DYLC) chip capable of bud reorientation and concerted daughter dissection for replicative lifespan determination. Journal of Nanobiotechnology, 2022, 20, 171.	9.1	5
147	An interpretation of reverse current in metal/intrinsic diamond/semiconducting diamond junction diodes. Applied Surface Science, 2001, 171, 57-62.	6.1	4
148	Contact UV Lithography Simulation for Thick SU-8 Photoresist. , 2006, , .		4
149	A dynamic macromodel for distributed parameter magnetic microactuators. Chinese Physics B, 2008, 17, 1709-1715.	1.4	4
150	A nodal analysis model for the out-of-plane beamshape electrothermal microactuator. Microsystem Technologies, 2009, 15, 217-225.	2.0	4
151	A Modified 3D fast marching simulation for thick photoresists lithography. , 2011, , .		4
152	An online test structure for the thermal expansion coefficient of surface micromachined polysilicon beams by a pull-in approach. Journal of Micromechanics and Microengineering, 2012, 22, 055017.	2.6	4
153	Passive Wireless Hermetic Environment Monitoring System for Spray Painting Workshop. Sensors, 2016, 16, 1207.	3.8	4
154	Modelling and characterization of a robust, low-power and wide-range thermal wind sensor. Microsystem Technologies, 2017, 23, 5571-5585.	2.0	4
155	Modeling of the Effect of Process Variations on a Micromachined Doubly-Clamped Beam. Micromachines, 2017, 8, 81.	2.9	4
156	A Novel Measurement Method of Mechanical Properties for Individual Layers in Multilayered Thin Films. Micromachines, 2019, 10, 669.	2.9	4
157	Uncertainty quantification of MEMS devices with correlated random parameters. Microsystem Technologies, 2020, 26, 1689-1696.	2.0	4
158	An efficient <scp>electroâ€thermoâ€mechanical</scp> model for the analysis of Vâ€shaped thermal actuator connected with driven structures. International Journal of Numerical Modelling: Electronic Networks, Devices and Fields, 2021, 34, e2843.	1.9	4
159	Differential piezoresistive wind speed sensor on flexible substrate. Electronics Letters, 2020, 56, 201-203.	1.0	4
160	An efficient macro model for CMOS-MEMS thermal wind speed sensor. Journal of Micromechanics and Microengineering, 2020, 30, 125001.	2.6	4
161	Simulation and experiment of miniaturized housing structure for MEMS thermal wind sensors. Sensors and Actuators A: Physical, 2022, 333, 113297.	4.1	4
162	Analytic Model of Dual-Layer-Structure MEMS Thermal Wind Sensor With Increased Sensitivity. IEEE Transactions on Electron Devices, 2022, 69, 1341-1348.	3.0	4

#	Article	IF	CITATIONS
163	Rotational Speed Measurement Based on LC Wireless Sensors. Sensors, 2021, 21, 8055.	3.8	4
164	A novel bonding technology for GaAs sensors. Sensors and Actuators A: Physical, 1990, 21, 40-42.	4.1	3
165	GaAs piezoelectric modulated resistors. Sensors and Actuators A: Physical, 1993, 35, 247-254.	4.1	3
166	An interpretation of SiO2-induced emission instability in silicon field emitter. Applied Surface Science, 1998, 136, 36-40.	6.1	3
167	On-line extraction for thermal conductivity of surface-micromachined polysilicon thin films. , 0, , .		3
168	An atomic level model for silicon anisotropic etching processes: Cellular automaton simulation and experimental verification. Applied Physics Letters, 2007, 91, 174101.	3.3	3
169	Package Level Simulation and Verification of Microsystems. , 2007, , .		3
170	Wafer level packaging based on AU-AU bonding for a CMOS compatible thermal wind sensor. , 2011, , .		3
171	Fabrication of a push-pull type electrostatic comb-drive RF MEMS switch. , 2012, , .		3
172	H2O adsorption-induced curvature of a silicon nanocantilever based on a semi-continuum method. Applied Surface Science, 2013, 282, 662-671.	6.1	3
173	<i>In situ</i> test structures for the thermal expansion coefficient and residual stress of polysilicon thin films. Journal of Micromechanics and Microengineering, 2013, 23, 075019.	2.6	3
174	Development of a robust 2-D thermal wind sensor using glass reflow process for low power applications. , 2015, , .		3
175	A self-packaged self-heated thermal wind sensor with high reliability and low power consumption. , 2015, , .		3
176	A Micro-Test Structure for the Thermal Expansion Coefficient of Metal Materials. Micromachines, 2017, 8, 70.	2.9	3
177	Sensitivity Analysis of Micromachined Thermal Wind Sensor Based on Back Surface Sensing Mode. , 2018, , .		3
178	Annular-Encapsulation Packaging to Realize High-Performance MEMS Thermal Wind Sensor. , 2018, , .		3
179	Eight-trigram-inspired MEMS thermal wind sensor with improved accuracy. , 2018, , .		3
180	A 2D Waveguide Method for Lithography Simulation of Thick SU-8 Photoresist. Micromachines, 2020, 11, 972.	2.9	3

#	Article	IF	CITATIONS
181	Efficient system-level simulations of thermal wind sensors considering environmental factors. Journal of Micromechanics and Microengineering, 2022, 32, 085002.	2.6	3
182	Possible Current Oscillations in Field Emission from N-Type Silicon. Japanese Journal of Applied Physics, 1995, 34, L918-L920.	1.5	2
183	SPICE Model with Lumped Circuits for A Thermal Flow Sensor. , 2006, , .		2
184	A CMOS interdigital capacitive humidity sensor with polysilicon heaters. , 2010, , .		2
185	Complementary metal-oxide semiconductor compatible capacitive barometric pressure sensor. Journal of Micro/ Nanolithography, MEMS, and MOEMS, 2011, 10, 013018.	0.9	2
186	A hybrid model for the charging process of the amorphous SiO 2 film in radio frequency microelectromechanical system capacitive switches. Chinese Physics B, 2011, 20, 037701.	1.4	2
187	Micro-rotating structures for determining thermal expansion coefficients of polysilicon thin films. , 2012, , .		2
188	MEMS-Based Intraoperative Monitoring System for Improved Safety in Lumbar Surgery. IEEE Sensors Journal, 2013, 13, 1541-1548.	4.7	2
189	Three-dimensional modeling and simulation of the Bosch process with the level set method. , 2014, , .		2
190	A passive wireless integrated humidity sensor based on dual-layer spiral inductors. , 2014, , .		2
191	Effect of packaging asymmetry on the performance of a 2D MEMS thermal wind sensor with different heating geometries. , 2015, , .		2
192	Temperature dependence of the quality factor in LC-type passive wireless temperature sensors. , 2015, , .		2
193	Experiments and Solution of Asymmetry Effect for Mems Thermal wind Sensor. , 2019, , .		2
194	A Micromachined Thermal Wind Sensor. Micro/Nano Technologies, 2018, , 539-576.	0.1	2
195	Micromachined Humidity Sensors. Micro/Nano Technologies, 2018, , 787-816.	0.1	2
196	A simple C-V method for measuring minority lifetime of nonuniformly doped MOS structures. Solid-State Electronics, 1991, 34, 419-420.	1.4	1
197	Micro-electro-mechanical digital-to-analog converter based on a novel bimorph thermal actuator. , 0,		1
198	Coupled Fabrication Process Simulation and Mechanical Performance Analysis of Microstructures		1

Based on Cellular Automata. , 2006, , .

#	Article	IF	CITATIONS
199	Measurement of residual stress in multilayered thin films by a full-field optical method. , 2006, , .		1
200	Flip-chip on board packaging of a thermal wind sensor. , 2008, , .		1
201	A novel 2-D wind sensor with thermal feedback. , 2008, , .		1
202	A smart 2-D wind sensor with self-test function. , 2008, , .		1
203	Simulations, analysis and characterization of the development profiles for the thick SU-8 UV lithography process. , 2010, , .		1
204	A system level modeling for distributed RF MEMS devices considering thermally induced packaging effect. , 2011, , .		1
205	Detecting magnetic field direction by a micro beam operating in different vibration modes. Chinese Physics B, 2011, 20, 097101.	1.4	1
206	Animal experimental study on the nerve root retraction with a silicon pressure sensor. , 2011, , .		1
207	A memory and computation efficient three-dimensional simulation system for the UV lithography of thick SU-8 photoresists. , 2012, , .		1
208	Measurement of material properties for polysilicon thin films by an electrostatic force method. , 2012, , .		1
209	An equivalent-circuit method for coupled-field modeling of distributed RF MEMS devices and packages. , 2012, , .		1
210	Direct observation of blocked nanoscale surface evaporation on SiO2 nanodroplets. Applied Physics Letters, 2012, 101, 183114.	3.3	1
211	Three-dimensional simulation of surface topography evolution in the Bosch process by a level set method. Microsystem Technologies, 2015, 21, 1587-1593.	2.0	1
212	In-Situ Testing of the Thermal Diffusivity of Polysilicon Thin Films. Micromachines, 2016, 7, 174.	2.9	1
213	A high linearity capacitive temperature sensor fabricated by metalmumps process. , 2016, , .		1
214	Effects of environmental media on the transmission of an inductive link in wireless microsystems. Frontiers of Mechanical Engineering, 2017, 12, 554-556.	4.3	1
215	RF MEMS Switch. Toxinology, 2017, , 1-38.	0.2	1
216	Design and optimization of thermal-mechanical reliability of a TSV 3D Packaged Thermal Wind Sensor. , 2017, , .		1

#	Article	IF	CITATIONS
217	Micromachined Humidity Sensors. Toxinology, 2017, , 1-30.	0.2	1
218	Modeling and Simulation of SU-8 Thick Photoresist Lithography. Toxinology, 2017, , 1-31.	0.2	1
219	RF MEMS Switch. Micro/Nano Technologies, 2018, , 1039-1076.	0.1	1
220	Experimental Study of a Dual-Mode Control MEMS Wind Sensor with High Accuracy. , 2018, , .		1
221	Ultra-remote LC Sensor Based on The Broken PT-Symmetry. , 2019, , .		1
222	Enhancing LC Sensor Telemetry via Magnetic Resonance Coupling. , 2019, , .		1
223	A Fast Response Flexible Humidity Sensor based on PTFE Micropore Substrate. , 2019, , .		1
224	Influence of Aerodynamic Housing on the Performance of MEMS Wind Sensor. , 2020, , .		1
225	Flexible LC-Type Wind Speed Sensor With Its Readout Circuit. IEEE Sensors Journal, 2021, 21, 19857-19862.	4.7	1
226	A Micromachined Thermal Wind Sensor. Toxinology, 2017, , 1-43.	0.2	1
227	Biasedâ€voltage controlled thinning for bonded siliconâ€onâ€insulator wafers. Applied Physics Letters, 1995, 66, 2990-2991.	3.3	0
228	Influence of silicon doping density on vacuum field emission triode at high frequency range. Journal of Infrared, Millimeter and Terahertz Waves, 1996, 17, 1447-1456.	0.6	0
229	Analytical piezoelectric charge densities in GaAs MESFETs. IEEE Transactions on Electron Devices, 1996, 43, 509-510.	3.0	Ο
230	M-Test Method for Measuring Mechanical Property of Multi-layer in MEMS. International Journal of Nonlinear Sciences and Numerical Simulation, 2002, 3, .	1.0	0
231	An in-situ technique for measuring Young's modulus and residual stress of each layer for multi-layer film. , 0, , .		Ο
232	A Novel Model for Surface Evolvement and Footing Effect Simulations in DRIE Fabrications. , 2006, , .		0
233	Plasma Etching Process Simulation for MEMS and IC Fabrication based on a Cellular Automata Method. , 2006, , .		0
234	Numerical study on photoresist etching processes based on a cellular automata model. Science in China Series D: Earth Sciences, 2007, 50, 57-68.	0.9	0

#	Article	IF	CITATIONS
235	Anisotropic etching of silicon in alkaline solutions : Microscopic activation energy calculations for silicon atoms and its simulation applications. , 2008, , .		Ο
236	Detection of stiction of suspending structures in MEMS by A Laser Doppler Vibrometer systems. , 2008, , .		0
237	Modeling and simulation of a novel capacitive temperature sensor. , 2008, , .		0
238	Effect of temperature and elastic constant correction on piezoresistivity of silicon nanobeams. , 2009, , .		0
239	The effect from the substrate reflection to the inclined UV lithography of SU-8 photoresist. Proceedings of SPIE, 2009, , .	0.8	0
240	Behavior simulation for electrically actuated bow-tie shaped fixed-fixed beams based on nodal analysis method. , 2009, , .		0
241	An electrical probe for measuring thermal expansion coefficients of micromachined polysilicon thin films. , 2010, , .		0
242	Elasticity of si calculated with a lattice dynamics model. , 2010, , .		0
243	Design of a capacitive pressure sensor based on flip-chip packaging technology. , 2010, , .		0
244	Theoretical modeling of thermal expansion of crystalline silicon by using the strain phonon spectra. , 2011, , .		0
245	Measurement of elastic modulus and residual stress of individual layers for composite films by resonant frequency of MEMS structures. , 2012, , .		Ο
246	Modeling of H <inf>2</inf> O adsorption-induced curvature of a nanocantilever. , 2012, , .		0
247	C-V characterization of the piezocapacitive effect with a microfabricated cantilever. , 2012, , .		Ο
248	An in-situ measurement method for thermally induced packaging stress in distributed RF MEMS Phase Shifters. , 2013, , .		0
249	Size-dependent thermal expansion properties of Silicon nanowires. , 2013, , .		Ο
250	Wide span thermal wind sensor system with dual chips. , 2013, , .		0
251	First-principles study on the electro-mechanical coupling of the Si/Ge core-shell nanowires. , 2013, , .		0
252	Development of a novel bidirectional electrothermal actuator and its application to RF MEMS switch.		0

^{, 2014, , .}

#	Article	IF	CITATIONS
253	A new method for measuring the temperature-dependent dielectric constant of the PDMS fluids. , 2015, , .		0
254	Towards an LC passive wireless sensor platform. , 2017, , .		0
255	On-line Test Microstructures of the Mechanical Properties for Micromachined Multilayered Films. Toxinology, 2017, , 1-40.	0.2	0
256	Online Test Microstructures of the Thermophysical Properties of MEMS Conducting Films. Toxinology, 2017, , 1-67.	0.2	0
257	Modeling and Simulation of SU-8 Thick Photoresist Lithography. Micro/Nano Technologies, 2018, , 67-97.	0.1	Ο
258	Reliability Optimization of a 3D Packaged Micro-machined Wind Sensor. , 2018, , .		0
259	Readout Distance Enhancement of the Passive Wireless Multi-Parameter Sensing System Using a Repeater Coil. Journal of Sensors, 2018, 2018, 1-6.	1.1	Ο
260	Implementation of Four-parameter LC Sensing Through Symmetric Dual-Resonant Circuit. , 2019, , .		0
261	Compact Mems Thermal Wind Sensor Using Dual Polysilicon Layers with Improved Accuracy. , 2019, , .		Ο
262	Modeling and Simulation of Silicon Anisotropic Etching. Toxinology, 2017, , 1-23.	0.2	0
263	Modeling and Simulation of Silicon Anisotropic Etching. Micro/Nano Technologies, 2018, , 3-25.	0.1	Ο
264	Online Test Microstructures of the Thermophysical Properties of MEMS Conducting Films. Micro/Nano Technologies, 2018, , 237-302.	0.1	0
265	Online Test Microstructures of the Mechanical Properties for Micromachined Multilayered Films. Micro/Nano Technologies, 2018, , 197-235.	0.1	Ο
266	Passive and Wireless Anemometer Based on Inductor Bending Effect. Journal of Microelectromechanical Systems, 2022, 31, 3-5.	2.5	0